Available online at www.sciencedirect.com
ScienceDirect
International Journal of Thermal Sciences 48 (2009) 322–330
International Journal of Thermal Sciences
www.elsevier.com/locate/ijts

Prandtl/Schmidt number effect on temperature distribution in a generic combustor

Lei-Yong Jiang *, Ian Campbell

Gas Turbine Laboratory, Institute for Aerospace Research, National Research Council Canada, 1200 Montreal Road, M-10, Ottawa, Ontario, Canada, K1A 0R6

Received 25 September 2007; received in revised form 10 March 2008; accepted 11 March 2008

Available online 15 April 2008

Abstract

As a benchmarking of turbulence scalar transfer modeling, the effect of Prandtl/Schmidt number on the temperature field of a diffusion flame model combustor has been investigated. Some of the numerical results, obtained from the eddy dissipation combustion model with the turbulent Prandtl/Schmidt number varying from 0.25 to 0.85, are presented and compared with a comprehensive experimental database. It is found that the turbulent Prandtl/Schmidt number has significant effect on the predicted temperature field in the combustion chamber. This is also true for the temperature profile along the combustor wall. In contrast, its effect on the velocity field is insignificant in the range considered. With the optimized turbulent Prandtl/Schmidt number, both velocity and temperature fields can be reasonably and quantitatively predicted. For the present configuration and operating conditions, the optimal Prandtl/Schmidt number is 0.5, and lower than the typical used value of ∼0.7. This study suggests that the current method for scalar transfer modeling in turbulent reacting flows should be improved and new approaches should be developed.

Keywords: Turbulence scalar transfer; Combustor modeling; Schmidt number; Prandtl number; Reynolds analogy

1. Introduction

Today, numerical simulation has become an essential tool in the development of advanced gas turbine combustors. Accurate temperature prediction at the combustor wall and exit is vital to gas turbine engineers since poor temperature profiles can significantly reduce the lifetime of the combustor and the turbine behind it.

In almost all turbulent reacting flow Reynolds-averaged Navier–Stokes (RANS) simulations, the turbulent Prandtl (Pr_t) and Schmidt (Sc_t) numbers are used to determine the turbulence scalar transfers (mixture fraction, species and energy or temperature) based on the modeled momentum transfer. For most practical turbulent reacting flows, Pr_t can be considered equal to Sc_t, that is, $Le = 1$ [1–3]. This has been verified by many experimental studies in heated and/or tracer jet flows [1].

Numerous studies were made concerning Pr_t and Sc_t in the last century, particularly in the period of 1930s–1970s [1,2,4]. Hinze [1] reviewed a large number of experimental measurements on Pr_t or Sc_t in pipe, duct and boundary-layer flows, and pointed out that Pr_t or Sc_t varied from 0.6 to 0.8. Recently, based on their velocity and concentration half-width measurements in axisymmetric jets of air and helium, Panchapakesan and Lumley [5] obtained an average value of 0.7 for Sc_t. Yimer et al. [6], combining a well-defined velocity measurement and passive scalar measurement in axisymmetric jets, calculated the radial distribution of Sc_t in the fully developed region without the intermittency effect. The results showed Sc_t varying from 0.62 to 0.82.

All the above experimental results suggest that an average value of $Pr_t = Sc_t = \sim 0.7$ should be used in numerical simulations. This has been applied to many numerical studies, such as jet flows [7,8] and gas turbine combustor modeling [9,10]. However, low Pr_t and Sc_t numbers from 0.20 to 0.5 have been used by a number of authors for simulating kerosene-fueled gas turbine combustors. Crocker et al. [11] modeled an entire combustor from the compressor diffuser exit to the turbine

* Corresponding author. Tel.: +1 613 993 9235; fax: +1 613 952 7677.
E-mail address: leiyong.jiang@nrc-cnrc.gc.ca (L.-Y. Jiang).

1290-0729/$ – see front matter
doi:10.1016/j.ijthermalsci.2008.03.014

Nomenclature

C_p	specific heat at constant pressure
D	molecular diffusivity
f	mixture fraction
f''	fluctuating component of mixture fraction
H	total enthalpy
h	heat transfer coefficient
k	turbulence kinetic energy
Le	Lewis number, Sc_t/Pr_t
M	molecular weight
p	probability density function
Pr_t	turbulent Prandtl number
r	radial coordinate
S	energy source term
Sc_t	turbulent Schmidt number
St	Stanton number
T	temperature
U	mean axial velocity
U_∞	free stream velocity
u	axial velocity component
$\mathbf{V}$	velocity vector
$\mathbf{v}''$	fluctuating velocity vector
v	radial velocity component
$u''v''$	turbulence shear stress
x	coordinate along the combustor axis of symmetry
Y	species mass fraction
y^+	non-dimensional parameter, $\sqrt{\tau_w/\rho}y/\upsilon$
y	distance to the wall boundary
Z	mass fraction of element
ε	turbulence dissipation rate
ω	species source term
ν	stoichiometric coefficient
υ	kinematic viscosity
ρ	density
Γ_t	turbulent Prandtl or Schmidt number
μ_t	turbulent viscosity
μ	molecular viscosity
ϕ	species mass fraction, mixture fraction, or total enthalpy
ϕ''	scalar fluctuating component
τ_w	wall shear stress

Greek symbols

Γ_t	turbulent Prandtl or Schmidt number
ε	turbulence dissipation rate
μ	molecular viscosity
μ_t	turbulent viscosity
ρ	density
τ_w	wall shear stress
υ	kinematic viscosity
ϕ	species mass fraction, mixture fraction, or total enthalpy
ϕ''	scalar fluctuation component
ϕ	species mass fraction, density or temperature
ω	species source term

inlet, including the air split and liner wall temperature prediction. The value of Pr_t and Sc_t was set to 0.25 since this low value consistently demonstrated better agreement with combustor fuel/air mixing results. Kaaling et al. [12] studied five RQL (rich burn, quick quench, lean burn) low-emission combustor designs both experimentally and numerically. The CFD calculations were calibrated against the coherent anti-Stokes Raman scattering (CARS) measurements, and good agreement was found by using $Pr_t = Sc_t = 0.2$. Large eddy simulations (LES) of a Rolls-Royce production gas turbine combustor were carried by Cannon et al. [13], where $Pr_t = Sc_t = 0.5$ was used. Moreover, the effect of Schmidt number on turbulence scalar mixing of a gaseous jet issued into a cross airflow was investigated by He et al. [14]. In comparison with the available experimental data, $Pr_t = Sc_t = 0.2$ was recommended.

To provide a benchmark database for the evaluation and development of various physical models, a series of experiments were performed in a diffusion flame model combustor at the National Research Council of Canada. The comprehensive experimental results make the present study possible.

The objective of the present work is to determine if such a low value of Pr_t and Sc_t is physically realistic, and to provide some recommendations for scalar transfer modeling in turbulent reacting flows. Since the model combustor geometry is much simpler than practical combustors, its boundary conditions are well defined and a comprehensive experimental database is available, and hence the assessment of the above issue is more reliable.

2. Experimental measurements

Fig. 1 is a schematic of the model combustor, including the fuel and air inlets, combustion chamber and contracted exhaust section, where the dimensions are in mm. Air entered the combustion chamber around a disc flame-holder, while fuel was fed through the center of the bluff body. The test rig was mounted on a three-axis traversing unit with a repeatability of ± 100 μm. The fuel used in the experiments was commercial grade propane, and dry air was delivered from a shop air supply. Both air and fuel flows were controlled by Sierra Side-Trak mass-flow controllers with 2% accuracy in full scale (fuel 100 l/min and air 2550 l/min).

To reduce the heat losses through walls, a 25.4-mm thick fibre blanket of Al_2O_3 was wrapped around the combustion chamber. Four narrow slots were cut into the blanket to allow appropriate physical and optical access to the chamber interior. Interchangeable sets of stainless steel and fused silica windows were used for physical probing using gas sampling probes, radiometers and thermocouples, as well as for optical probing using the laser Doppler anemometer (LDA). The viewing area of the windows measured 17 mm in width and 344 mm in length.

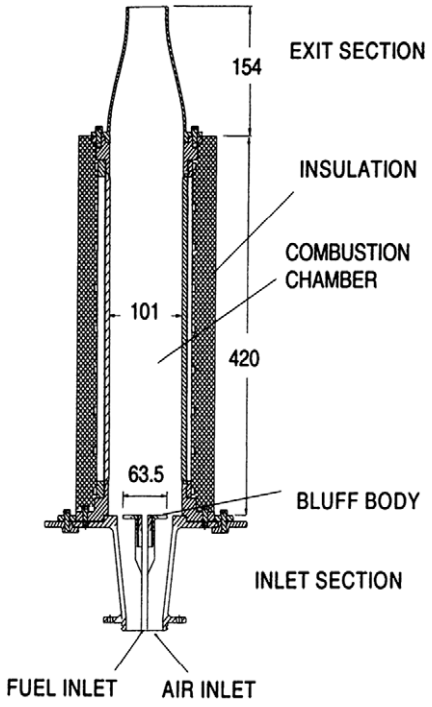

Fig. 1. The model combustor.

Measurements of velocity were made using both a 2- and 3-component LDA system operating in the back scattering mode. In the lower section of the combustion chamber, limited optical access forced the use of a single fibre optic head to measure axial and tangential velocities. In the upper section of the chamber, a complete three-component LDA system was used. Gas temperatures were acquired using an uncoated 250-μm diameter S-type thermocouple supported by a twin-bore ceramic tube. Thermocouples embedded in and flush with the combustor wall were used to measure the wall temperature. Gas species measurements were made with a sampling probe connected to a Varian Model 3400 Gas Chromatograph. The major species measured were CO, CO_2, H_2O and C_3H_8. Details of the experimental setup and measurements can be found in Ref. [15].

3. Numerical simulations

Axisymmetric, steady, turbulent, reacting flows were considered in the present study, and a commercial software package, Fluent, was used as the platform for all numerical simulations. The computational domain, governing equations, selected physical models, boundary conditions and solution methods are described in the following sub-sections.

3.1. Computational domain

The computational domain covered the entire combustor flow field from the fuel and air inlets to the exhaust exit (see Fig. 1). Moreover, the internal and external conjugate heat transfers from the combustion mixture to the flame-holder body and insulation walls were also modeled.

Since the flow field was axisymmetric, 2D quadrilateral meshes were used. Fine grids were laid behind the flame-holder in the combustion chamber in order to resolve the recirculation region. Fine grids were also generated in the shear layers between the recirculation region and fuel and air jets, as well as in the gap between the flame-holder edge and air inlet chamber wall. Coarse grids were used for the solid stainless steel and ceramic walls. A total number of 74,100 elements were used for most of the simulations. The skewness was less than 0.2 in the flow-field domain and the aspect ratio was less than 12 for 99.5% of the elements. Efforts were made to keep the wall parameter $y^+(\sqrt{\tau_w/\rho}\,y/\upsilon)$ in the desired range (30 to 60). A number of meshes were tested to ensure the mesh independence of the numerical solutions.

3.2. Governing equations

The first-moment Favre-averaged conservation equations for mass, momentum, species, mixture fraction and total enthalpy, may be expressed in a coordinate-free form as [16,17],

$$\nabla \bullet (\bar{\rho}\tilde{\mathbf{V}}) = 0 \tag{1}$$

$$\nabla \bullet (\bar{\rho}\tilde{\mathbf{V}}\tilde{V}) = -\nabla \bar{p} + \nabla \bullet \mathbf{T} - \nabla \bullet (\overline{\rho \mathbf{v}''\mathbf{v}''}) \tag{2}$$

$$\nabla \bullet (\bar{\rho}\tilde{\mathbf{V}}\tilde{Y}_i) = \nabla \bullet (\bar{\rho} D_i \nabla \tilde{Y}_i) - \nabla \bullet (\overline{\rho \mathbf{v}'' Y_i''}) + \omega_i \tag{3}$$

$$\nabla \bullet (\bar{\rho}\tilde{\mathbf{V}}\tilde{f}) = \nabla \bullet (\bar{\rho} D \nabla \tilde{f}) - \nabla \bullet (\overline{\rho \mathbf{v}'' f''}) \tag{4}$$

$$\nabla \bullet (\bar{\rho}\tilde{\mathbf{V}}\tilde{H}) = \nabla \bullet \left(\frac{\mu}{Pr_l}\nabla \tilde{H}\right) - \nabla \bullet (\overline{\rho \mathbf{v}'' H''}) + S_H \tag{5}$$

In the above equations, $\bar{\rho}$ represents mean density, $\tilde{\mathbf{V}}$ is mean velocity vector, $\mathbf{v}''$ stands for fluctuation velocity vector, the viscous stress tensor $\mathbf{T} = \mu[\nabla\tilde{\mathbf{V}} + (\nabla\tilde{\mathbf{V}})^T] - \frac{2}{3}\mu\nabla \bullet \tilde{\mathbf{V}}\,\mathbf{I}$ with $\mathbf{I}$ a unit tensor, $\overline{\rho\mathbf{v}''\mathbf{v}''}$ denotes Reynolds stresses, Y_i is the mass fraction of the ith species, f stands for mixture fraction, H denotes total enthalpy, and D and Pr_l represent molecular diffusivity and Prandtl number, respectively.

For closure of the above equations, the species source term, ω_i in Eq. (3) is obtained from a selected combustion model. The energy source term, S_H in Eq. (5) includes viscous heating and radiation heat transfer that is obtained by a radiation model. As mentioned earlier, Reynolds stresses, $\overline{\rho\mathbf{v}''\mathbf{v}''}$ or turbulence momentum transfer in Eq. (2) are modeled by a selected turbulence model, while $\overline{\rho\mathbf{v}''Y''}$, $\overline{\rho\mathbf{v}''f''}$, $\overline{\rho\mathbf{v}''H''}$ or turbulence scalar transfers in Eqs. (3)–(5) are calculated based on the modeled momentum transfer.

3.3. Turbulence modeling

The previous benchmarking on turbulence modeling [18] has illustrated superiority of the Reynolds stress model (RSM) over three other popular two-equation eddy-viscosity models. Therefore, the RSM was chosen to model turbulence momentum transfer in the current study. Detailed description and derivation are beyond the scope of the present paper and can be found in Ref. [19].

For axisymmetric flows as in the present case, four transportation equations of Reynolds stresses, $\overline{\rho\mathbf{v}''\mathbf{v}''}$ along with the turbulence dissipation rate equation are solved in the combustor

flow field. From the solutions of Reynolds stresses and dissipation rate, the turbulent viscosity (momentum transfer coefficient) is then computed,

$$\mu_t = \overline{\rho} C_\mu \tilde{k}^2/\tilde{\varepsilon} \tag{6}$$

where $C_\mu = 0.09$, and k and ε are turbulence kinetic energy and dissipation rate, respectively.

With Pr_t and Sc_t, the turbulence scalar transfers are determined from the following expression,

$$-\nabla \bullet \overline{\rho \mathbf{v}'' \phi''} = \nabla \bullet \left(\frac{\mu_t}{\Gamma_t} \nabla \tilde{\phi} \right) \tag{7}$$

where ϕ stands for species mass fraction, mixture fraction or total enthalpy, and Γ_t represents Pr_t or Sc_t. Note that in Eq. (7), the turbulence scalar transfer coefficients, μ_t/Γ_t, are simply the products of the turbulence momentum transfer coefficient (μ_t) and $1/\Gamma_t$. In addition, it should be understood that in the present study, the isotropic turbulence transfer (coefficient) assumption is abandoned in momentum transfer; however, it is still used for turbulence scalar transfers.

3.4. Combustion modeling

Three combustion models were used in the investigation, i.e., the eddy-dissipation (EDS), probability density function (PDF), and laminar flamelet model. The trends and magnitudes among these three models are similar. In this paper, some of the numerical results from the EDS combustion model are presented and discussed. For completeness, the optimal Pr_t and Sc_t numbers for all three models are provided at the end.

The EDS model is based on the work of Magnussen and Hjertager [20], which has been widely accepted in diffusion flame modeling [21]. The reaction rate is governed by turbulent mixing, or the large-eddy mixing time scale, k/ε. The net reaction rate of species "i" is given by the smaller of the following two expressions in kg/m^3 s,

$$R_i = \nu_i M_i A \overline{\rho} \frac{\tilde{\varepsilon}}{\tilde{k}} \min\left[\frac{\tilde{Y}_{C_3H_8}}{\nu_{C_3H_8} M_{C_3H_8}}, \frac{\tilde{Y}_{O_2}}{\nu_{O_2} M_{O_2}} \right] \tag{8}$$

$$R_i = \nu_i M_i A B \overline{\rho} \frac{\tilde{\varepsilon}}{\tilde{k}} \frac{(\tilde{Y}_{CO_2} + \tilde{Y}_{H_2O})}{(\nu_{CO_2} M_{CO_2} + \nu_{H_2O} M_{H_2O})} \tag{9}$$

where ν stands for the stoichiometric coefficient, M represents the molecular weight, and the empirical constants, $A = 4.0$ and $B = 0.5$. The description of the PDF and propane-air flamelet model used in the study can be found in elsewhere [22].

3.5. Other physical models

To account for the radiation heat transfer between the gas mixture and combustion chamber walls, the discrete ordinates radiation model [23] was employed. The absorption coefficient of gaseous mixture was determined from local species mass fractions in the flow. An absorption coefficient of 0.5 was set for the stainless steel wall and disc flame-holder. An enhanced wall boundary treatment was applied at all internal walls. In this approach, a two-layer model is combined with wall functions, and the viscous and fully turbulent regions are smoothly blended.

Polynomials used to calculate the specific heat of species as a function of temperature were determined from Ref. [24], where the chemical dissociation was considered. For other thermal properties of the mixture such as molecular viscosity, thermal conductivity, diffusivity and absorption coefficient, the values for air at 900 K were used. The thermal conductivity was 25 W/m K for the stainless steel, and 0.1 W/m K for the ceramic insulation.

3.6. Boundary conditions

The fuel mass flow rate was 16.2 g/s and the airflow rate was 550 g/s, and then the corresponding overall equivalence ratio was 0.46. The Reynolds number based on the air entry velocity and flame-holder diameter was 1.9×10^5. An estimated turbulence intensity of 10% and hydraulic diameters were used to estimate Reynolds stress components and turbulence dissipation rate at the fuel and air inlets. For both flows, the inlet temperature was 293 K.

The wall boundary temperatures were defined based on the experimental measurements. A room temperature of 293 K was assigned to the walls of the inlet section, as well as the upstream edges of the combustion chamber and ceramic insulation walls. A linear temperature profile from 294 to 405 K was specified along the outer boundary of the ceramic insulation wall. The temperature of the outer boundary of the exit section was set to 960 K. The same temperature was assigned to the downstream edge of the combustion chamber wall because its heat resistance was much smaller than the ceramic insulation. A linear temperature profile from 960 to 405 K was assigned to the downstream edge of the insulation wall. Finally, the pressure at the combustor exit was set to the atmospheric value.

3.7. Solution methods

A segregated solver with a second-order accurate scheme was used to resolve the flow field. A node-based method for derivatives was chosen in order to maintain numerical stability as Γ_t close to 0.25. At convergence, the normalized residuals of flow variables were about or less than 10^{-5} in all test cases. The monitored axial velocities at two points in the shear layer downstream of the flame-holder remained unchanged at least for the first four digits. A 4-node LINUX cluster, 64-bit, 2.6 GHz, dual CPU and 8 GB RAM for each node, was used to perform all simulations.

4. Results and discussion

Numerical simulations were performed with Γ_t varying from 0.25 to 0.85, and a large amount of data were processed and analyzed. As stated earlier, only some of the results obtained from the EDS combustion model are presented here. In the following subsections, the velocity field results are first presented, then

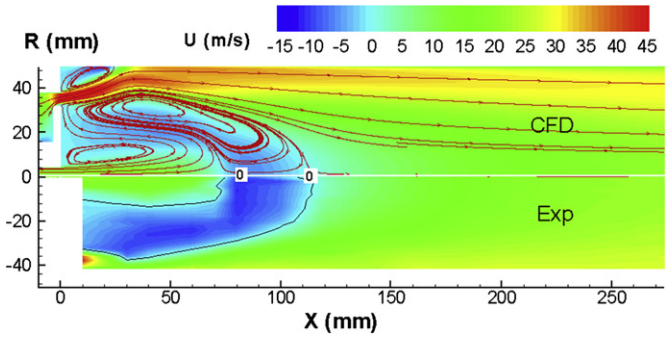

Fig. 2. Axial velocity contours and flow path-lines, $\Gamma_t = 0.85$.

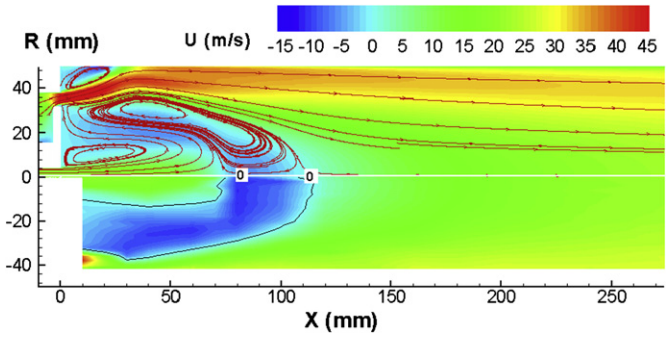

Fig. 3. Axial velocity contours and flow path-lines, $\Gamma_t = 0.50$.

the temperature results are discussed, and finally the current approach to turbulence scalar transfer modeling is assessed.

4.1. Velocity distributions

The upper half of Fig. 2 shows the axial velocity contours and flow path-lines with $\Gamma_t = 0.85$. The lower half of the figure presents the experimental data with the zero axial velocity lines specified. Agreement between the numerical predictions and experimental results for the flow patterns in the combustion chamber is excellent. Two recirculation zones are formed behind the flame-holder although, in the experimental case, the central recirculation zone is not completely resolved and no flow path-lines are drawn due to the limited data points. It is significant that both reattachment points or lengths of the two recirculation zones are excellently predicted. The central recirculation zone created by the fuel jet is completely confined within the annular recirculation zone generated by the annular air jet. This implies that the transportation of fuel into the flow field is realized by laminar and turbulent diffusion only through the annular recirculation zone, which poses a challenge to turbulent reacting flow simulations.

Although turbulence scalar transfers are calculated based on the turbulence momentum transfer, the former also affects the latter since they are coupled. The effect of Γ_t on the velocity field is illustrated in Figs. 3 and 4 for $\Gamma_t = 0.50$ and 0.25, respectively. Difference in the flow field between $\Gamma_t = 0.85$ and $\Gamma_t = 0.50$ is minor. For $\Gamma_t = 0.25$, the length and volume of the annular recirculation zone are slightly reduced in comparison with those in Figs. 2 and 3. The numerical results indicate that

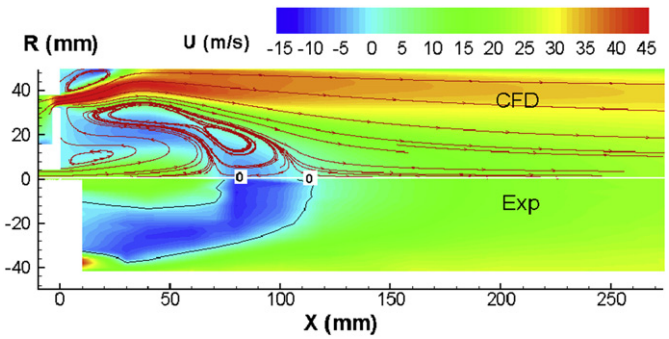

Fig. 4. Axial velocity contours and flow path-lines, $\Gamma_t = 0.25$.

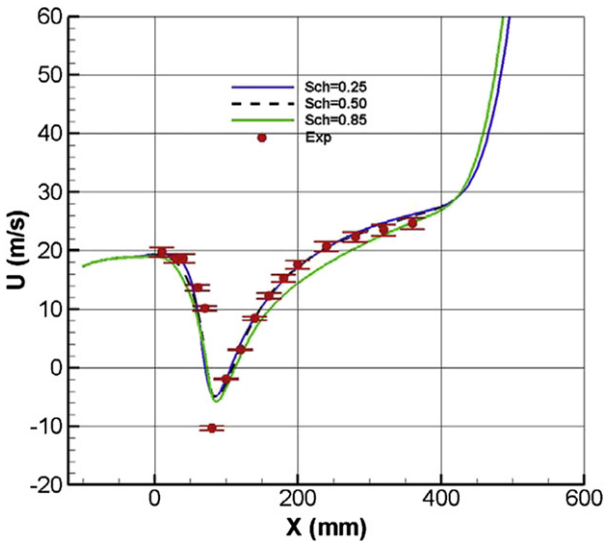

Fig. 5. Axial velocities along the combustor centerline. (For colors see the web version of this article.)

in the range of Γ_t studied, the Γ_t effect on the velocity field is limited, particularly for $\Gamma_t > 0.35$.

Fig. 5 gives the predicted axial velocity profiles along the combustor centerline, where they are compared with the experimental measurements. Superimposed in the figure, in red, are the estimated error bars of 2%. The numerical results show good agreement with the experimental data, except that the peak value of negative velocities is under-predicted. The effect of Γ_t variation from 0.85 to 0.25 on the centerline velocity profile is insignificant.

The predicted axial velocity profiles at five cross-sections, two inside the recirculation region, one close to the stagnation point, and the last two located downstream of the recirculation region, are presented in Fig. 6, and qualitatively compared with the experimental results. In general, the profiles are predicted reasonably well except in the local regions at three middle sections, where the discrepancies increase as Γ_t decreases. It should be noted that the flow field is complex at these three sections, which represents a difficult task to numerical simulations.

Fig. 7 shows quantitative comparisons of turbulence kinetic energy between the numerical and experimental results at four cross-sections from $x = 60$ to 240 mm. Error bars in the figure

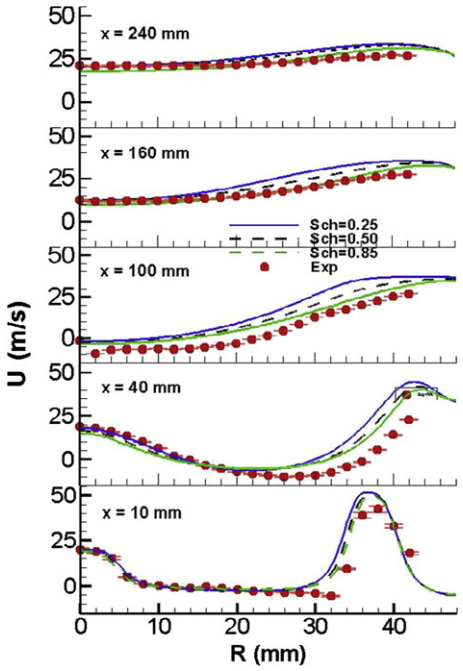

Fig. 6. Axial velocity profiles at sections, $x = 10$ to 240 mm.

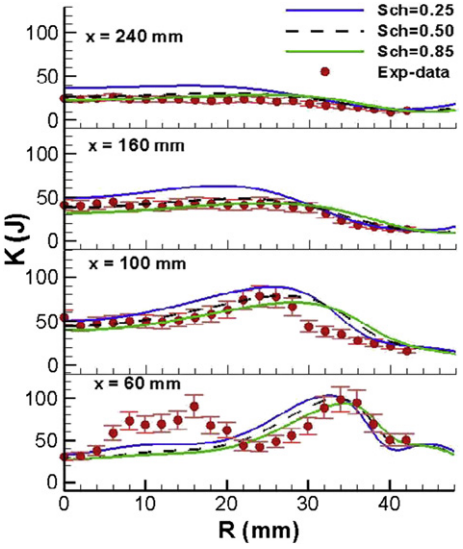

Fig. 7. Turbulence kinetic energy profiles at sections, $x = 60$ to 240 mm.

represent 8% of measurement accuracy. The trends and magnitudes are predicted reasonably well, except for the magnitudes at two downstream sections with $\Gamma_t = 0.25$. As observed at section $x = 60$ mm, the numerical results fail to pick up the first bump of the experimental data, which appears in the region of $r \approx 7$–17 mm. Note that in this region, the axial velocity changes its direction (from positive to negative). The anticipated reasons are twofold: (1) the maximum magnitude of negative axial velocity is under-predicted (see Fig. 5); (2) the predicted small recirculation zone does not completely match the experimental data (see Figs. 2–4). That is, the numerical axial velocity gradient in this region is much lower than that from the measurements, and therefore the numerical simulation does not show the first bump.

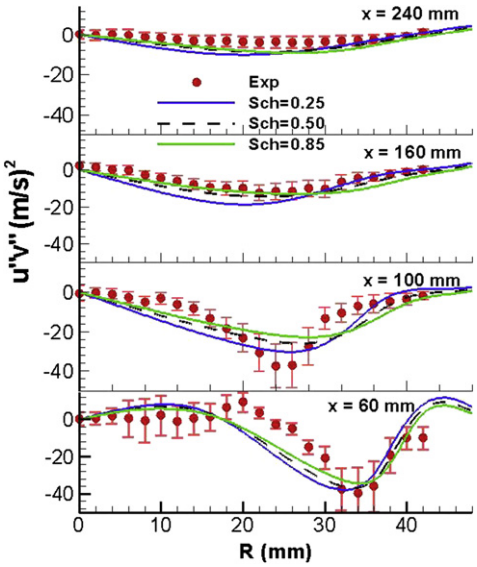

Fig. 8. Turbulence shear stress profiles at sections, $x = 60$ to 240 mm.

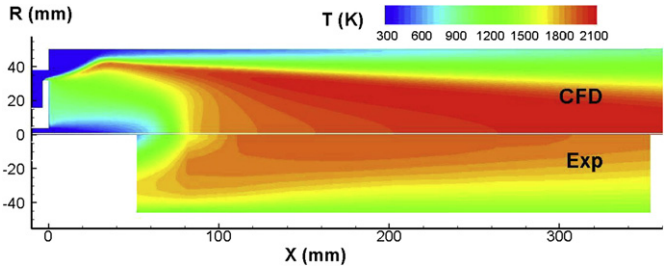

Fig. 9. Temperature contours, $\Gamma_t = 0.85$.

Fig. 8 compares the numerical results of the turbulence shear stress, $\overline{\rho u'' v''}/\bar{\rho}$ with the measured experimental data at four cross-sections. Here the estimated measurement accuracy is about 12%. The turbulence shear stress is of primary interest for momentum transport in turbulent flows, particularly in shear flows. Again, the trends and magnitudes are reasonably well predicted, and the effect of Γ_t variation is insignificant, particularly in comparison with the measurement error. At section $x = 60$ mm, discrepancies between the numerical and experimental results are observed in the middle region ($r \approx 20$–30 mm). The reason is expected to be similar to that for Fig. 7. In the corresponding region, the predicted velocities show less variation than the experimental measurements.

The above numerical results indicate that the effect of Γ_t variation on the predicted velocity field is limited, and the velocity fields predicted by the RSM turbulence model agree reasonably well with the experimental data for $\Gamma_t > 0.4$. With the adequate prediction of momentum transfer or velocity field, the current approach to turbulence scalar transfer modeling (or temperature modeling) can be evaluated properly.

4.2. Temperature distributions

The temperature contours for $\Gamma_t = 0.85$, 0.5 and 0.25 are presented and compared with the experimental database in Figs. 9–11, respectively. As expected, the temperature in the

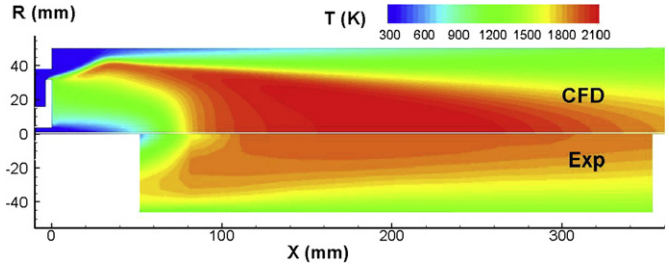

Fig. 10. Temperature contours, $\Gamma_t = 0.50$.

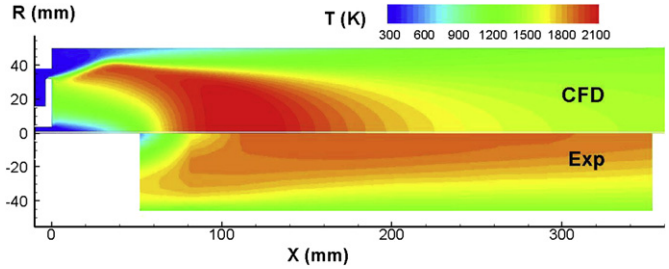

Fig. 11. Temperature contours, $\Gamma_t = 0.25$.

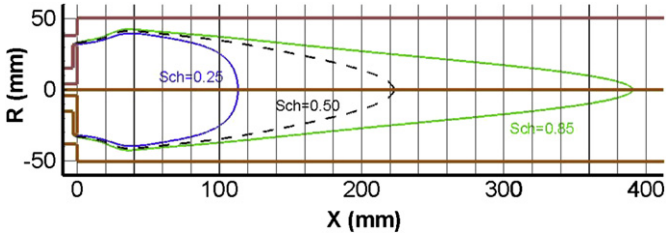

Fig. 12. Variation of predicted flame length with Γ_t.

recirculation region is relatively uniform due to strong turbulent mixing. Intense chemical reaction takes place around the envelope of the annular recirculation zone. In comparison with the experimental data, the high temperature region is shifted downstream for $\Gamma_t = 0.85$, significantly reduced and shifted upstream for $\Gamma_t = 0.25$, and best predicted with $\Gamma_t = 0.50$. That is, the high temperature region moves upstream and becomes smaller with Γ_t decreasing. This is because the turbulence transfer of fuel into the air flow and then chemical reaction are accelerated as Γ_t decreases. In general, the overall temperature patterns and high temperature region are best predicted with $\Gamma_t = 0.50$ although the temperature contours near the recirculation region are slightly better predicted with $\Gamma_t = 0.85$ than those with $\Gamma_t = 0.50$.

In Figs. 9–11, it is found that the predicted temperature in the high temperature region is higher than the measured values. The maximum difference is about 170 K. The main reason may be that the temperature was measured by a 0.25-mm diameter thermocouple, as mentioned earlier. Owing to the radiation and conduction losses from the thermocouple, the measurement error could exceed 100 K over regions where the gas temperature was high and the flow velocity was low [25].

The effect of Γ_t on the predicted flame length is illustrated in Fig. 12, where the flame region is represented by the stoichiometric line of the mean mixture fraction, i.e., $\tilde{f} = 0.063$. The

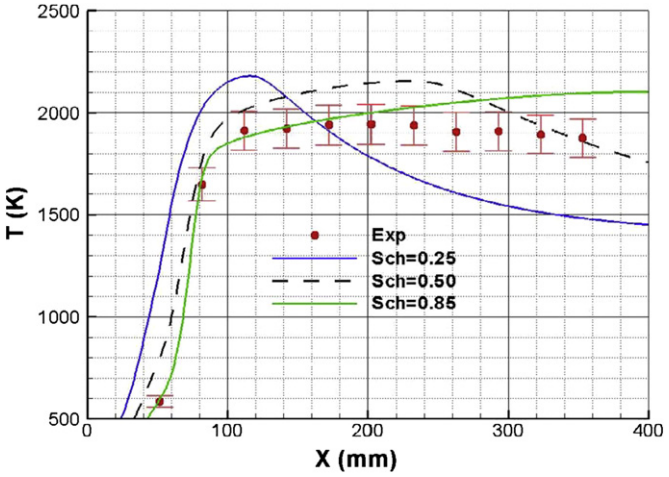

Fig. 13. Temperature profiles along the combustor centerline.

Γ_t effect on the flame length and region is obvious. As Γ_t decreases from 0.85 to 0.25, both the flame length and region are significantly reduced, and the flame length shrinks about three times, from 390 to 113 mm.

The predicted temperature profiles along the combustor centerline are compared with the experimental data in Fig. 13, where the measurement error is about 5%. In the upstream region ($x < \sim 80$ mm), the effect of Γ_t is limited; the numerical results for $\Gamma_t = 0.50$ and 0.85 agree well with the experimental data although the results for $\Gamma_t = 0.85$ are slightly better than those for $\Gamma_t = 0.50$ and relatively large deviations are found for $\Gamma_t = 0.25$. In contrast, the effect of Γ_t is obvious in the downstream region. $\Gamma_t = 0.50$ gives the best results although the predicted profile shows a peak in the middle portion, while the measurements tend to be flat.

It is believed that in the upstream region the fuel distribution or chemical reaction is mainly determined by the location and size of the annular recirculation zone, which is formed by complex flow interactions among the central fuel jet, annular air flow and two recirculation zones. However, in the downstream region, the turbulent diffusion or transfer plays a dominant role in the fuel spreading away from the axis of symmetry, where the flow path-lines are almost parallel to each other as shown in Figs. 2–4.

Fig. 14 presents the temperature profiles for $\Gamma_t = 0.85$, 0.50 and 0.25 at five cross-sections from $x = 52$ to 233 mm. As expected, at all sections, as Γ_t decreases the temperature profiles become more flat, i.e., the fuel spreading becomes faster. The numerical results from $\Gamma_t = 0.50$ agree reasonably well with the experimental results, except for the regions near the combustor wall. In these near-wall regions, the temperature is under-predicted, which may suggest that the fuel spreading is under-predicted in these local regions. Poor performance is observed for $\Gamma_t = 0.25$ at most sections. Strong effects of Γ_t are observed at all sections.

The variation of combustor wall temperature profiles with Γ_t is shown in Fig. 15. The numerical results are compared with the measured wall temperature, where the measurement error is about 2.5%. As expected, the predicted wall temperature in-

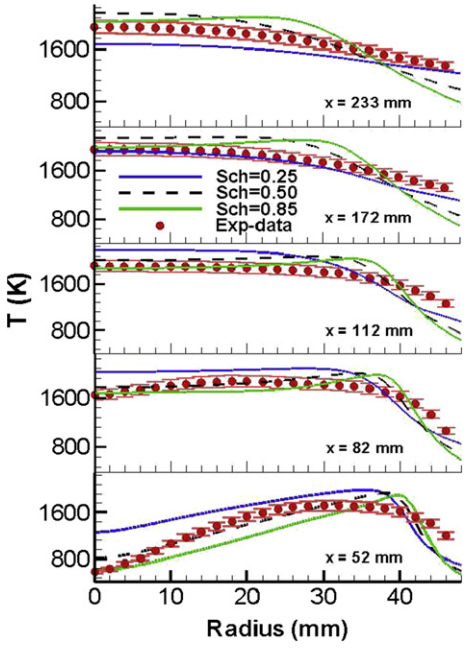

Fig. 14. Temperature profiles at sections $x = 52$–233 mm.

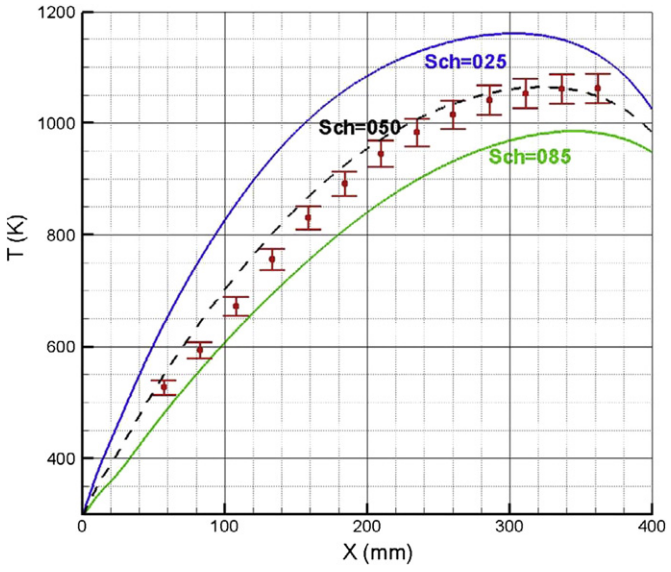

Fig. 15. Temperature profiles along the combustor wall.

Table 1
Optimal Prandtl and Schmidt number

	EDS	PDF	Flamelet
T-chamber	0.50	0.50	0.50
T-wall	0.50–0.55	0.55	0.40

creases as Γ_t decreases. The results with $\Gamma_t = 0.50$ show the best agreement with the measurements although the wall temperature is somewhat over-predicted in the upstream region.

Finally, for comparison, the optimized Γ_t numbers for the three combustion models are given in the following table. As shown in Table 1, the optimal Γ_t for the temperature prediction inside the combustion chamber is 0.50 for all three combustion models; however, it varies from 0.40 to 0.55 for the wall temperature prediction. This implies that the combustion model has some effect on the near-wall temperature distribution.

4.3. Discussion

As found from this study, the optimal Γ_t number for temperature prediction inside the combustor is 0.50. This number is different from 0.25 in [11], 0.20 in [12] for kerosene-fueled gas turbine combustor modeling, and 0.20 for a cross-jet flow simulation [14]. However, it is the same as used in [13] for a Rolls-Royce gas turbine combustor LES study.

All these examples imply two important observations. First, the optimized Γ_t number is lower than the commonly accepted values of ~0.7. In the sense of the average relative strength between the turbulence momentum and scalar transfers, a low value of Γ_t number is a true physical phenomenon. Second, the optimal Γ_t number is most likely dependent on the combustor configuration and possibly operating conditions. That is, a priori optimization is required in order to reasonably predict temperature distribution inside combustors. Obviously, this type of prior optimization is not practical in the real world.

The reasons for the above observations can be explained theoretically and experimentally. An analogy between the wall shear and heat flux in boundary layers was first postulated by Osborne Reynolds over a century ago [26]. This original hypothesis has been considerably amended and applied to computational simulations of general turbulent reacting or mixing flows since 1970s.

Theoretically, the rationale and limitation of the Reynolds analogy approach could be revealed by reducing the conservation equations (2)–(5) to axisymmetric steady boundary flows and neglecting the streamwise pressure gradient, molecular viscous terms, and source terms. Then the following equations are obtained,

$$\bar{\rho}\tilde{u}\frac{\partial \tilde{u}}{\partial x} + \bar{\rho}\tilde{v}\frac{\partial \tilde{u}}{\partial r} = \frac{1}{r}\frac{\partial}{\partial r}\left(r\mu_t\frac{\partial \tilde{u}}{\partial r}\right) \tag{10}$$

$$\bar{\rho}\tilde{u}\frac{\partial \tilde{\phi}}{\partial x} + \bar{\rho}\tilde{v}\frac{\partial \tilde{\phi}}{\partial r} = \frac{1}{r}\frac{\partial}{\partial r}\left(r\frac{\mu_t}{\Gamma_t}\frac{\partial \tilde{\phi}}{\partial r}\right) \tag{11}$$

where the turbulent viscosity concept is applied to both streamwise momentum and scalar transfers. With $\Gamma_t = 1$, the two equations are identical. This means that under practical boundary conditions, the flow variable fields are similar. For wall boundary flows with relatively large radius with respect to boundary thickness, the original form of the Reynolds analogy can be deduced [31],

$$\frac{2St}{c_f} = \frac{(h/\rho C_p U_\infty)}{(\tau_w/\rho U_\infty^2)} \approx 1 \tag{12}$$

where St is the Stanton number and c_f stands for skin friction coefficient. It is clear that Eqs. (10)–(12) are only valid for boundary layer flows where a number of terms are neglected. Certainly, its application to complex turbulent reacting flows is questionable.

Experimentally, the commonly accepted values of Γ_t (~0.7) are measured from fully developed boundary or pipe flows [1, 2,4–6], and they may not be suitable for practical turbulent

reacting flows. Recently a number of authors [27–30] have experimentally discovered that this idea is no longer applicable to disturbed turbulent thermal boundary flows.

In summary, applications of the concept, calculating turbulence scalar transfers based on the modeled momentum transfer and Prandtl/Schmidt number, are limited. For accurate prediction of scalar transfers in turbulent reacting flows without prior optimization, this concept should be improved and new approaches should be developed.

5. Conclusions

The effect of turbulent Prandtl/Schmidt number on the flow field of a propane diffusion flame combustor with interior and exterior conjugate heat transfers has been numerically studied. Presented and discussed in this paper are some of the results obtained from the eddy dissipation combustion model with turbulent Prandtl/Schmidt number varying from 0.25 to 0.85.

In comparison with the comprehensive experimental database, it is found that the Γ_t number has insignificant effect on the velocity field. In contrast, it shows strong effects on the temperature field, particularly downstream in the combustion chamber. It is also true for the temperature profile along the combustor wall.

For the present combustor configuration and operating conditions, the optimal Γ_t is 0.5 for temperature prediction inside the combustor for all three combustion models. With $\Gamma_t = 0.50$, both velocity and temperature fields are reasonably well predicted, except in some local and near-wall regions. The optimal Γ_t varies from 0.40 to 0.55 for the combustor wall temperature prediction.

Finally, the rationale and limitation of current turbulence scalar transfer modeling are discussed. For accurate temperature prediction in turbulent reacting flows without tuning turbulent Pr_t and Sc_t number, the current concept should be improved and new approaches should be studied.

Acknowledgements

The authors are grateful to Dr. Bill Wallace for his valuable comments and suggestions during the preparation of this paper. Also the authors want to express many thanks to Miss Abdelmesih Gewana (co-op student) for her assistance in the post-processing of numerical and experimental results.

References

[1] J.O. Hinze, in: Turbulence, The McGraw-Hill Book Company Inc., New York, 1987, pp. 372–753.
[2] F.M. White, in: Heat and Mass Transfer, Addison-Wesley Publishing Company, New York, 1988, pp. 320–641.
[3] P.A. Libby, F.A. Williams, Fundamental aspects and a review, in: P.A. Libby, F.A. Williams (Eds.), Turbulent Reacting Flows, Academic Press, New York, 1994, pp. 1–61.
[4] E.R.G. Eckert, R.M. Drake Jr., Analysis of Heat and Mass Transfer, McGraw-Hill Book Company, New York, 1972.
[5] N.R. Panchapakesan, J.L. Lumley, Turbulence measurements in axisymmetric jets of air and helium, Part 2, Helium jet, Journal of Fluid Mechanics 246 (1993) 225–247.
[6] I. Yimer, I. Campbell, L.Y. Jiang, Estimation of the turbulent Schmidt number from experimental profiles of axial velocity and concentration for high-Reynolds-number jet flows, Canadian Aeronautics and Space Journal 48 (3) (2002) 195–200.
[7] C.L. Lubbers, G. Brethouwer, B.J. Boersma, Simulation of the mixing of a passive scalar in a round turbulent jet, Fluid Dynamics Research 28 (2001) 189–208.
[8] D.B. Spalding, Concentration fluctuations in a round turbulent free jet, Chem. Eng. Sci. 26 (1971) 95–107.
[9] X.S. Bai, L. Fuchs, Sensitivity study of turbulent reacting flow modeling in gas turbine combustors, AIAA Journal 33 (10) (1995) 1857–1864.
[10] M.K. Lai, CFD analysis of liquid spray combustion in a gas turbine combustor, in: The IGTI Expo, Orlando, FL, 1997, 1997-GT-309.
[11] D.S. Crocker, D. Nickolaus, C.E. Smith, CFD modelling of a gas turbine combustor from compressor exit to turbine inlet, in: The IGTI Expo 1998, Stockholm, Sweden, 1998, 1998-GT-184.
[12] H. Kaaling, R. Ryden, Y. Bouchie, D. Ansart, P. Magre, C. Guin, RQL combustor development including design, CFD calculations, CARS measurements and combustion tests, in: The 13th International Symposium Air Breathing Engines, Chattanooga, TN, USA, 1997, ISABE 97-7069.
[13] S.M. Cannon, C.E. Smith, M.S. Anand, LES predictions of combustor emissions in an aero gas turbine engine, in: 39th AIAA/ASME/SAE/ASEE Joint Propulsion Conference and Exhibit, Huntsville, Alabama, USA, 2003, AIAA-2003-4521.
[14] G. He, Y. Guo, A.T. Hsu, The effect of Schmidt number on turbulent scalar mixing in a jet-in-crossing flow, International Journal of Heat and Mass Transfer 42 (1999) 3727–3738.
[15] I. Campbell, D.L. Logan, An experimental study of a combusting flow past a confined bluff body, Combustion Institute, Canadian Section, Halifax, Canada, 1997.
[16] J.H. Ferziger, M. Peric, in: Computational Methods for Fluid Dynamics, Springer-Verlag, New York, 2002, pp. 1–10.
[17] Fluent Inc., Fluent 6.2 documentation, 10 Cavendish Court, Lebanon, NH 03766, USA, 2006.
[18] L.Y. Jiang, I. Campbell, Turbulence modeling in a model combustor, the IGTI Expo, Reno-Tahoe, Nevada, USA, 2005, 2005-GT-68403.
[19] B.E. Launder, G.J. Reece, W. Rodi, Progress in the development of a Reynolds-stress turbulence closure, J. Fluid Mech. 68 (1975) 537–566.
[20] B.F. Magnussen, B.H. Hjertager, On mathematical models of turbulent combustion with special emphasis on soot formation and combustion, in: 16th Symposium on Combustion (International), 1976.
[21] R.W. Bilger, Turbulent diffusion flames, annular review, Fluid Mechanics 21 (101) (1989) 101–135.
[22] L.Y. Jiang, I. Campbell, K. Su, A critical evaluation of combustion modeling in a model combustor, in: The Canadian 12th Annual Computational Fluid Dynamics Conference, Ottawa, Canada, 2004.
[23] G.D. Raithby, E.H. Chui, A finite-volume method for predicting a radiant heat transfer in enclosures with participating media, Journal of Heat Transfer 112 (1990) 415–423.
[24] J.W. Rose, J.R. Cooper, Technical Data on Fuel, John Wiley & Sons, New York, 1977.
[25] J.P. Sislian, L.Y. Jiang, R.A. Cusworth, Laser Doppler velocimetry investigation of the turbulence structure of axisymmetric diffusion flames, Prog. in Energy and Combustion Science 14 (2) (1988) 99–146.
[26] O. Reynolds, On the extent and action of the heating surface for steam boilers, Manchester Lit. Phil. 14 (1874) 7–12.
[27] K.S. Choi, D.M. Orchard, Turbulence management using riblets for heat and momentum transfer, Experimental Thermal and Fluid Science 15 (1997) 109–124.
[28] F. de Souza, J. Delville, J. Lewalle, J.P. Bonnet, Larger scale coherent structures in a turbulent boundary layer interacting with a cylinder wake, Experimental Thermal and Fluid Science 19 (1999) 204–213.
[29] J.C. Vogel, L.K. Eaton, Combined heat transfer and fluid dynamic measurements downstream of a backward-facing step, Journal of Heat Transfer 107 (1985) 922–929.
[30] E.D. John, J.O. Keller, Time-resolved gas temperature in the oscillating turbulent flow of a pulse combustor pipe, Combustion and Flame 80 (1990) 358–370.
[31] J. Bons, A critical assessment of Reynolds analogy for turbine flows, Transactions of the ASME, Journal of Heat Transfer 127 (2005) 472–485.